Journal of Hazardous Materials 161 (2009) 396–401

Contents lists available at ScienceDirect

Journal of Hazardous Materials

journal homepage: www.elsevier.com/locate/jhazmat

(Bi, C and N) codoped TiO_2 nanoparticles

Kangle Lv, Housong Zuo, Jie Sun, Kejian Deng*, Songcui Liu, Xiaofang Li, Duoyuan Wang

Key Laboratory of Catalysis and Materials Science of the State Ethic Affairs Commission & Ministry of Education, South-Central University for Nationalities, Wuhan 430074, China

ARTICLE INFO

Article history:
Received 6 July 2007
Received in revised form 4 March 2008
Accepted 27 March 2008
Available online 1 April 2008

Keywords:
Titanium dioxide
Photocatalytic degradation
Dope
Bismuth

ABSTRACT

Bi, C and N codoped TiO_2 photocatalysts were prepared by doping TiO_2 with $BiCl_3$ and KSCN in a sol–gel process (denoted as (Bi,SCN)-TiO_2). The catalyst samples were then characterized by XRD, TEM, diffuse reflectance spectra (DRS), XPS, FT-IR and N_2 sorption. Bi, C and N elements were detected both by XPS and elemental analysis, while S element was not found, suggesting that SCN^- group may have decomposed during the sol–gel process. The effects of the doping on the properties and photocatalytic activity of the TiO_2 were investigated. It was found that the cation and the anion affected the properties of TiO_2 differently. The optical absorption onset of TiO_2 red shifted in the presence of Bi^{3+}, while long tail occurred in the presence of SCN^-. The order of photoreactivity for TiO_2 samples was as follow: (Bi,SCN)-TiO_2 > Bi-TiO_2 > undoped TiO_2 > p25 TiO_2, whatever under UV or visible light illumination. The high photoreactivity of the doped TiO_2 was also discussed.

1. Introduction

A great deal of effort has been devoted in recent years to developing heterogeneous photocatalysts with high activities for environmental applications, such as air purification, water disinfection, hazardous waste remediation, and water purification [1,2]. Among various oxide semiconductor photocatalysts, titania has proven to be the most suitable for environmental applications for its chemical inertness, strong oxidizing power, cost effectiveness, and long-term stability [3,4].

The primary event occurring on the illuminated TiO_2 is the generation of e_{cb}^- and h_{vb}^+. In these reactions, the organic pollutants are oxidized by the photogenerated holes or by reactive oxygen species such as $OH^\bullet$ and O_2^- radicals formed on the irradiated TiO_2 surface. However, a problem in the application of TiO_2 as a photocatalyst is the large band gap energy, i.e. anatase only shows photocatalytic activity under UV-light irradiation of wavelengths <387 nm, corresponding to its band gap value of 3.2 eV.

Many studies have revealed that doping TiO_2 with nonmetal atoms, such as N [5], S [6], C [7], I [8], Br and Cl [9] shifts the optical absorption edge of TiO_2 to lower energies, thereby increasing the photoactivities. Another way of extending the TiO_2 spectral response and of improving its photoreactivity is doped with transition metals. Doping of transition metal ions including Cr [10], V [11] and Fe [12] have been investigated. Recently, we found that the photoreactivity of TiO_2 was greatly improved when doping with Bi [13]. Choi et al. [14] found that the photoreactivity of doped TiO_2 appears to be a complex function of the dopant concentration, the energy level of dopants within the TiO_2 lattice, their d electronic configuration, the distribution of dopants, the electron donor concentration, and the light intensity.

However, the effect of codoping by both cation and anion on the photocatalytic activity was seldom reported. Zhao et al. studied the TiO_2 doping with both a nonmetal element, boron, and a metal oxide, Ni_2O_3 [15]. They found that incorporation of B into TiO_2 extended the spectral response to the visible region and that the photocatalytic activity was greatly enhanced as it was further loaded with Ni_2O_3.

Recently, a number of Bi-based photocatalysts, such as $NaBiO_3$ [16], Bi_3O_4Cl [17], $Bi_4Ti_3O_{12}$ [18] and Bi_2WO_4 [3], were synthesized; these materials showed high photocatalytic activities even under visible light irradiation. It seems that bismuth maybe a proper candidate dopant element to extend the TiO_2 spectral response and thus to improve its photoreactivity. Another goal of the paper is to study the synergistic effects of codoping by both cation and anion on the photocatalytic activity of TiO_2. Here we report on doped TiO_2 with both Bi^{3+} and SCN^- by a simple method of modified sol–gel synthesis.

2. Experimental

2.1. Catalyst synthesis

Titanium *n*-butoxide (TTBO), KSCN, $BiCl_3$ and phenol were obtained from Shanghai. Chemical Co., China. The target dye pollutants, RhB (Fig. 1), was obtained from Acros Chem. Co. Commercial

* Corresponding author. Fax: +86 27 67842752.
E-mail address: Dengkj@scuec.edu.cn (K. Deng).

0304-3894/$ – see front matter © 2008 Elsevier B.V. All rights reserved.
doi:10.1016/j.jhazmat.2008.03.111

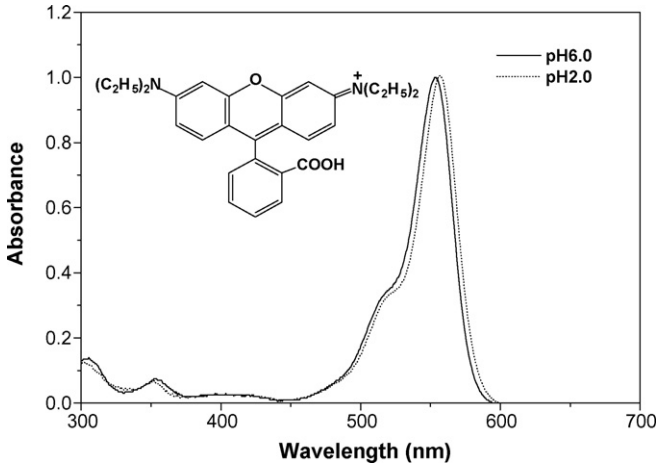

Fig. 1. Structure and electronic spectrum of rhodamine B (RhB).

P25 (Degussa, 50 m^2/g, 80% anatase and 20% rutile) was used as reference sample. Doubly distilled water was used throughout this study, and the pH of the solution was adjusted by diluted aqueous solutions of $HClO_4$ and NaOH.

The catalyst (Bi,SCN)-TiO_2, were prepared by the sol–gel method. In a typical preparation procedure, 10 ml TTBO was added dropwise to another mixture consisting of 5 ml of acetic acid and 20 ml of anhydrous ethanol under vigorous stirring at room temperature, and then 20 ml ethanol containing 0.3 mmol $BiCl_3$ and 0.1 mmol KSCN was added dropwise to the solution. After that, 25 ml water was added to form a slurry. The slurry was transferred to a 100 ml autoclave fitted with Teflon liner. The autoclave was maintained at 180 °C for 14 h and then air cooled to room temperature. The gray precipitate was collected, washed with distilled water. To prevent from sintering, the catalysts were dried under infrared irradiation instead of calcinations. Pure TiO_2 (undoped TiO_2), SCN-doped (SCN-TiO_2) and Bi^{3+} doped TiO_2 (Bi-TiO_2) samples were synthesized using the same method except the addition of $BiCl_3$ and/or KSCN.

2.2. Catalyst characterizations

The X-ray diffraction (XRD) patterns obtained on a D8-advance X-ray diffractometer (German Bruker) using Cu Kα radiation at a scan rate of 0.02° S^{-1} were used to determine the crystallite size and identity. The acceleration voltage and the applied current were 200 kV and 20 mA, respectively. The average crystallite size of anatase was determined according to the Scherrer equation using FWHM data after correcting the instrumental broadening. UV–vis absorption spectra of TiO_2 powder were obtained for the dry-processed disk samples using a UV–vis spectrophotometer (Lambda, Bio 35, PE Co., U.S.A.). Absorption spectra were referenced to $BaSO_4$. X-ray photoelectron spectroscopy (XPS) measurement was done using Multilab 2000 XPS system with a monochromatic Mg Kα source and a charge neutralizer, all the binding energies were referenced to the C 1s peak at 284.4 eV of the surface adventitious carbon. Transmission electron microscopy (TEM, Tecnai G20, FEI Co., U.S.A.) with an acceleration voltage of 200 KeV was used to examine the morphology and particle size. FT-IR spectra were recorded on a NEXUIS-470 infrared spectrometer (Nicolet Co., U.S.A.). Nitrogen adsorption–desorption isotherms were collected on a Micrometrics ASAP2010 adsorption analyzer at −196 °C (77 K).

A Shimadzu AA-646 atomic absorption spectrophotometer equipped with a bismuth, hollow-cathode lamp was used to determination the concentration of Bi^{3+} in TiO_2 samples, and $BiCl_3$ was used to prepare the standard solutions. The following instrumental parameters were used: wavelength = 223 nm, slit = 0.2 nm and source = 5 mA.

2.3. Photoactivity measurement

The effect of pH on the degradation of the organic pollutants has been studied in our previous work, and lower pH (higher acidity) favors for the degradation of RhB [13]. The light source was a 500-W halogen lamp (Institute of Electric Light Source, Shanghai, China) and cutoff at 320 nm by the Pyrex-glass reactor, or equipped with a glass cutoff filter to completely remove any radiation below 420 nm to ensure illumination by visible light source only. Before light irradiation, 50 ml TiO_2 suspension (pH 2.0) containing RhB (1.0×10^{-4} mol/l) or phenol (2.0×10^{-4} mol/l) was first sonicated for 5 min, and shaken at a constant rate in the dark overnight. At given time intervals of illumination, a 3 ml aliquot was drawn, centrifuged, and 1.0 ml of the supernatant was diluted in a 10-ml flask for analysis. The structure and the electronic absorption spectra of RhB at pH 2.0 and pH 6.0 were shown in Fig. 1, and its absorption spectra showed little change at the solution pH ranged from 6.0 to 1.0.

The profile of photocatalytic degradation rate constants of RhB as a function of TiO_2 concentration showed that the optimum loading of TiO_2 was 0.9g/l [13]. Thus, this dosage of TiO_2 was used throughout the experiment and the solution pH was adjusted to 2.0 before irradiation. The analysis of RhB was performed using UV–vis spectrophotometer and the absorbance of the filtrate at 550 nm was measure to determinate the concentration change, while phenol was analysed using a Varian HPLC system consisted of a UVD 340S Diode Array detector with an intersil ODS-3C18 reverse column (5 μm, 250 mm × 4.6 mm).

3. Results and discussion

3.1. Measurements of XRD, TEM, DRS, XPS and FT-IR

XRD was usually used for identification of the crystal phase and to estimate the anatase to rutile ratio as well as the crystallite size of each of the phases present. The XRD peaks at around $2\theta = 25.25°$ (1 0 1) in the spectrum of TiO_2 are identified as the anatase form, whereas the XRD peaks at $2\theta = 27.42°$ (1 1 0) are taken as the rutile form [19]. Fig. 2 shows the XRD patterns of TiO_2. It could be seen that the prepared pure TiO_2 was of pure anatase form (Fig. 2b). However, the intensity of the peaks at $2\theta = 25.25°$ decreased sharply and three new peaks at $2\theta = 25.92$, 32.54 and

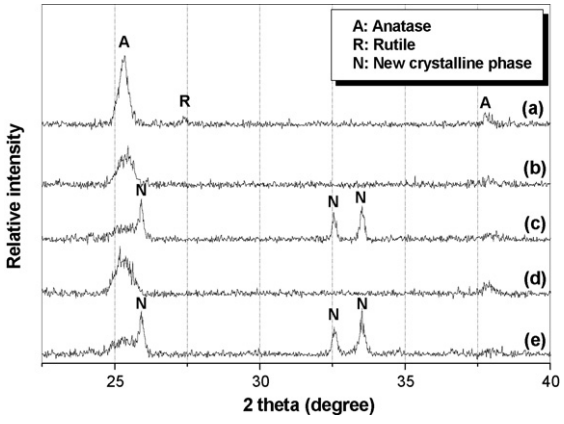

Fig. 2. XRD patterns of p25 TiO_2 (a), undoped-TiO_2 (b), Bi-TiO_2 (c), SCN^--TiO_2 (d) and (Bi,SCN)-TiO_2 (e).

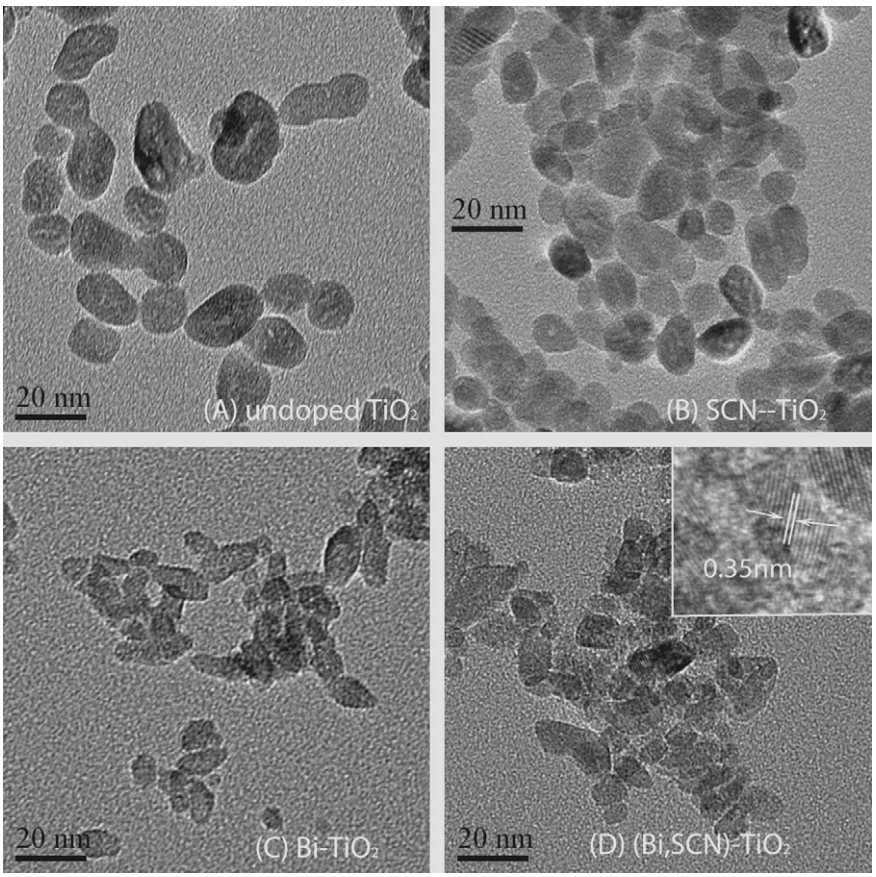

Fig. 3. Transmission electron micrographs of the prepared TiO_2 samples.

33.52° appeared simultaneously when it was doped with Bi^{3+} (Fig. 2c and e). It suggests that bismuth oxides or Bi_xTiO_y phases may be formed in the doped sample, or alternatively titanium atom may have substituted bismuth atom in the Bi_2O_3 lattice and a Ti—O—Bi bond may have formed. Both the formation of Ti—O—Bi bond and charge imbalance might greatly affect the chemical state of the Bi-TiO_2 surface. The average crystallite sizes of the TiO_2 samples were as follows: undoped TiO_2(12 nm), SCN-TiO_2(7.6 nm), Bi-TiO_2(4.9 nm) and (Bi,SCN)-TiO_2(3.0 nm), according to the Scherer equation. On doping with the anion, SCN^-, the XRD of the resulting material remained unchanged from the undoped sample and no other new diffraction peaks appeared (Fig. 2b and d), indicating no obvious change in the lattice of TiO_2 occurred on doping with the anion.

Fig. 3 shows the TEM photograph of the undoped TiO_2(A), SCN-TiO_2(B), Bi-TiO_2 (C), and (Bi,SCN)-TiO_2 (D). It is found that all the prepared TiO_2 nanoparticles appear similarly prism-shaped, with average particle size of about 10 nm.

Prior to evaluation of the photooxidation activity, the diffuse reflectance spectra (DRS) of the catalysts were measured, as shown in Fig. 4. Although the shape of the curve of the DRS spectrum of Bi-TiO_2 nanoparticles did not change after Bi^{3+} doping, it is found that the sharp decrease in DRS spectrum red shifted for about 15 nm (390 nm for undoped TiO_2 and 405 nm for Bi-TiO_2). The codoping of TiO_2 with SCN^- resulted in the sharp decrease red shifted for another 10 nm (up to 415 nm) and the long tail up to about 800 nm was obvious in DRS spectrum. The sharp decrease in the optical absorption spectrum is due to the band gap transition and the long tail is probably caused by the lattice defects, such as oxygen vacancies [16]. The optical band gaps, judging from the onset of the DRS, were estimated to be about 3.1 eV for Bi-TiO_2 and 3.0 eV for (Bi,SCN)-TiO_2 from the sharp decrease around 405 and 415 nm, respectively, due to the band gap transition [16]. Because (Bi,SCN)-TiO_2 absorbs a larger amount of visible light than Bi-TiO_2 and pure TiO_2, it could be a promising visible light photocatalyst.

The XPS spectra of (Bi,SCN)-TiO_2 nanoparticles surface are shown in Fig. 5. XPS peaks show that (Bi,SCN)-TiO_2 powder contains only Ti, Bi, O, C and a trace amount of N, and the signal of S was negligible. Through elemental analysis, the contents of C and N were 1.4% and 0.88%, respectively, while S element was not detected. These

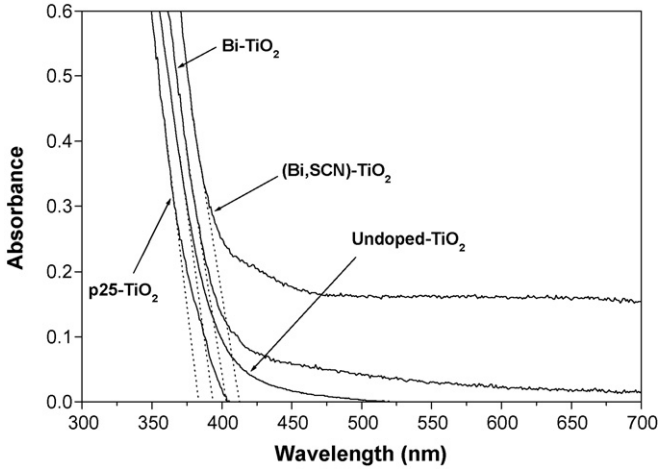

Fig. 4. Optical absorption spectra of p25 TiO_2, undoped TiO_2, Bi-TiO_2 and (Bi,SCN)-TiO_2.

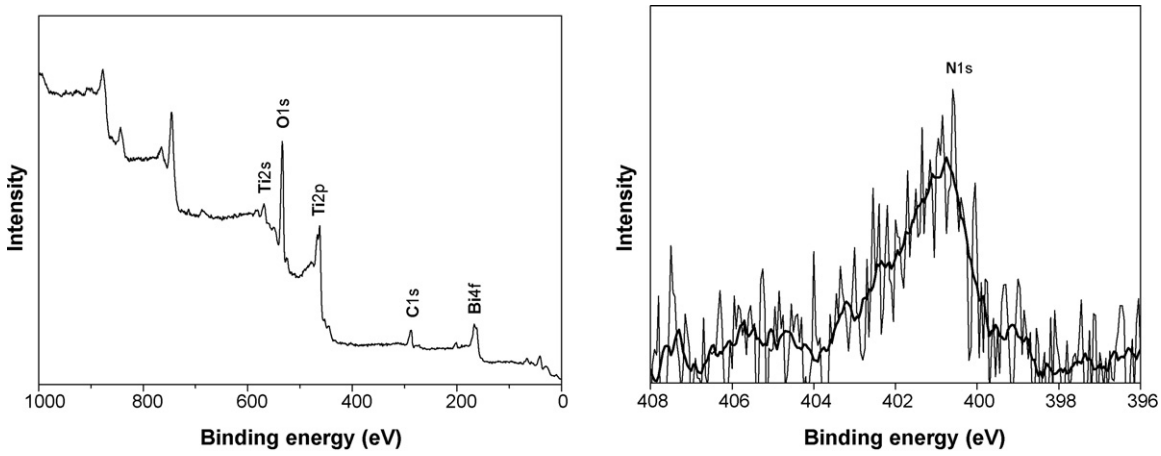

Fig. 5. XPS survey spectra of (Bi,SCN)-TiO_2 powders.

results suggest that SCN^- group may have decomposed during the sol–gel process. The content of bismuth was 1.8%, according to the atomic absorption spectroscopy (AAS).

The binding energy of Ti 2p is 459.0 eV, which is 0.8 eV higher than that of pure TiO_2 (458.2 eV) [20], due to the decrease of the electron density around the Ti^{4+} ions when doped with Bi^{3+} ions. At the same time, the binding energy of Bi 4f decreased to 160.03 eV, whereas the binding energy was reported to be 162.3 eV in bismuth trichloride [13]. These results infer that the Bi—O—Ti bonds may have been formed in the Bi-doped TiO_2 samples. The amount of bismuth atom is about at. 0.7%, according to XPS, which was consistent with the result measured by AAS (atomic absorption spectrum, with an error of ±2%).

Fig. 6 shows the IR spectra of TiO_2. The bands appearing at about 3425 cm^{-1} in Bi-TiO_2, corresponds to the stretching vibration of OH groups linking with titanium atoms (Ti-OH) and the band at 1630 cm^{-1} is the flexion vibration of OH group in adsorbed water [21,22]. These results confirm the presence of hydroxyl group in the structure of the samples. The adsorbed water and hydroxyl group are crucial to the photocatalytic reactions since they react with photo-excited holes on the catalyst surface to produce hydroxyl radicals, which are powerful oxidant. The small absorption band at 2974 cm^{-1} is probably caused by the stretching mode of unreacted ethoxy groups such as -Ti-OC_4H_9 [21]. The band centered at 1332 cm^{-1} is assigned to bending vibrations of C—H bond in the species linking -Ti-O-Ti- structural network. The intensity of the absorption at 1044 cm^{-1}, probably due to Bi-O-Ti stretching, increases with increasing Bi content in Bi-TiO_2 samples (not shown here). A new absorption peak appeared at 1523 cm^{-1} in (Bi,SCN)-TiO_2 sample, which was attributed to the N-O stretching vibrations. The peak at around 600 cm^{-1} was ascribed to absorption bands of Ti-O and O-Ti-O flexion vibration.

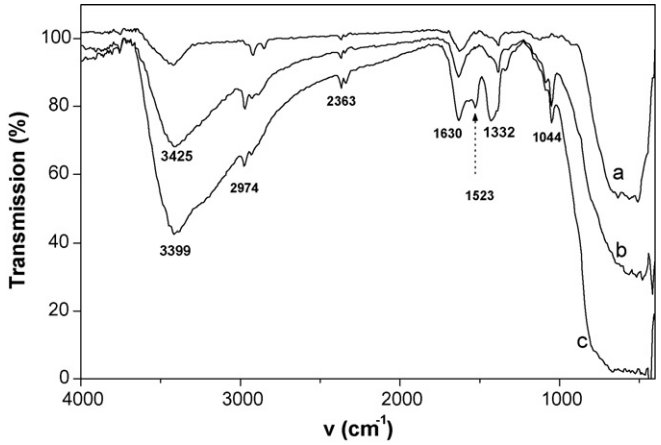

Fig. 6. IR spectra of p25 TiO_2 (a), Bi-TiO_2 (b) and (Bi,SCN)-TiO_2 (c) powders.

3.2. Nitrogen sorption

The Brunauer–Emmett–Teller (BET) specific surface areas, pore volumes of TiO_2 samples were summarized in Table 1. Compared with p25 TiO_2, the particle size of the prepared TiO_2 samples is much smaller, resulting in larger specific area. Small particle size could shorten the route for an electron migrates from the conduction band of the TiO_2 to its surface, while large surface area could provide more active sites and absorb more reactive species.

3.3. Measurement of photocatalytic activity

The adsorption of RhB (a cationic dye) on the surface of the TiO_2 catalyst is negligible due to the static repulse, as the particles are positively charged in acidic medium. To compare the catalytic activity of the catalysts, p25 TiO_2, undoped TiO_2, Bi-TiO_2 and (Bi,SCN)-TiO_2 were used in the 1.0×10^{-4} mol/l RhB, respectively, under UV and visible light illumination (Fig. 7). The kinetic data was well fitted by the apparent first-order rate equation, and the rate constants are listed in Table 2. Control experiment showed that the bleaching of RhB is very slow under UV light, with an apparent first-order rate constant of 0.081 h^{-1}. From the table, it can be seen that the order of photocatalytic activity of TiO_2 samples was as following: (Bi,SCN)-TiO_2 > Bi-TiO_2 > undoped TiO_2 > p25 TiO_2, whatever under UV or visible light illumination. (Bi,SCN)-TiO_2 is an efficient photocatalyst with an rate constant of 3.74 and 7.65 times higher than that of p25 TiO_2, under UV and visible light irradiation, respectively. Considering that RhB can also be degraded *via* photosensitization pathway, phenol, a colorless organic pollutant, was performed in p25 TiO_2 and (Bi,SCN)-TiO_2 suspensions under visible light illumination (Fig. 8). The degradation of phe-

Table 1
Textural properties of TiO_2 samples

Sample	A_{BET} (m^2/g)	V_{BJH} (cm^3/g)
Undoped TiO_2	106.1	0.156
Bi-TiO_2	146.2	0.228
(Bi,SCN)-TiO_2	161.8	0.237

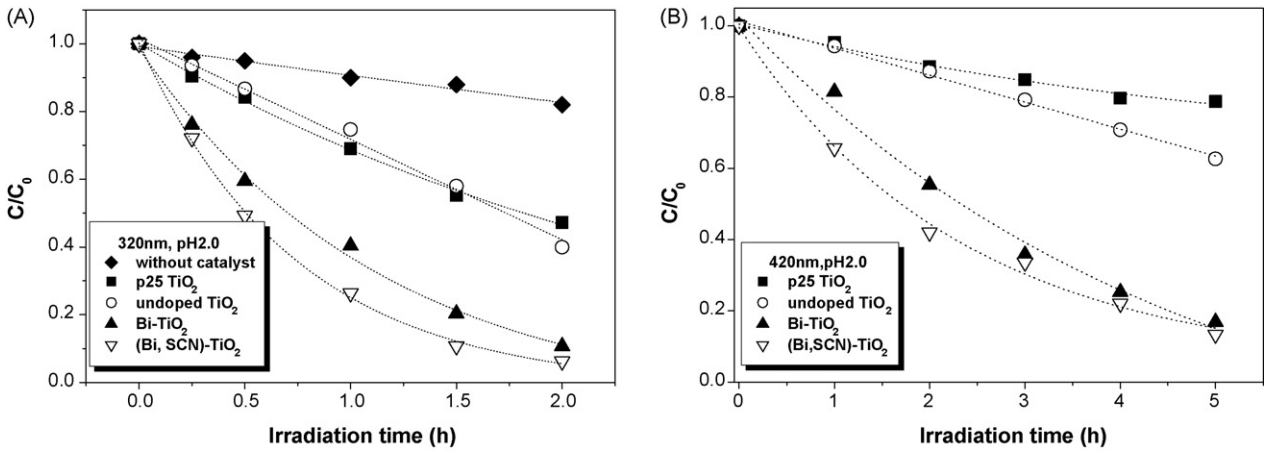

Fig. 7. Kinetics of degradation of RhB (1.0×10^{-4} M, pH 2.0) under UV ($\lambda > 320$ nm, A) and visible light ($\lambda > 420$ nm, B) irradiation.

nol was very slow in p25 TiO_2 suspension, with a rate constant of 0.0070 h^{-1}. However (Bi,SCN)-TiO_2 showed much higher photoactivity in the degradation of phenol, with a rate constant of 0.13 h^{-1} under the same condition. Thus, the photoreactivity of (Bi,SCN)-TiO_2 was 18.6 times higher than that of p25 TiO_2 under visible light irradiation.

During hydro-thermal treatment, guest metal oxides or dopants may react with titania to form new crystalline phases (Fig. 2). In the case of the Ti—Bi—O system, titania reacts with Bi^{3+} ions to produce Bi_xTiO_y, and then Bi_xTiO_y/TiO_2 heterojunction maybe formed. Heterojunctions of Cu_2O/TiO_2, Bi_2O3/TiO_2 and $ZnMn_2O_4/TiO_2$ has been studied in the literatures [23]. In case of $ZnMn_2O_4/TiO_2$ heterojunctions, it was found that electrons created on the conduction band of TiO_2 can be injected in the conduction band of $ZnMn_2O_4$, and holes generated on the TiO_2 valence band can be transferred to $ZnMn_2O_4$. Thus, the electrons and holes can be effectively separated and combination were greatly suppressed in heterojunctions after irradiation. Heterojunction effects between Bi_xTiO_y and TiO_2 may also exist and be responsible for the higher photoreactivity Bi-TiO_2. The related study is still in progress.

Table 2
Apparent first-order rate constants for the photocatalytic degradation of RhB on TiO_2 in water at pH 2.0 under UV ($\lambda > 320$ nm) or visible light ($\lambda > 420$ nm) illumination

Catalyst	$^{320}k_{first}$ (h^{-1})	^{320}R	$^{420}k_{first}$ (h^{-1})	^{420}R
p25 TiO_2	0.38	0.999	0.051	0.998
Undoped TiO_2	0.44	0.979	0.094	0.992
Bi-TiO_2	1.10	0.996	0.37	0.996
(Bi,SCN)-TiO_2	1.42	0.998	0.39	0.966

The kinetic data was fitted by the apparent first-order rate equation, $\ln(C/C_0) = k_{first} t$, where k_{first} is rate constant, C and C_0 are the concentration of RhB at irradiation time $t = 0$ and t, respectively. R is the linear regression coefficient.

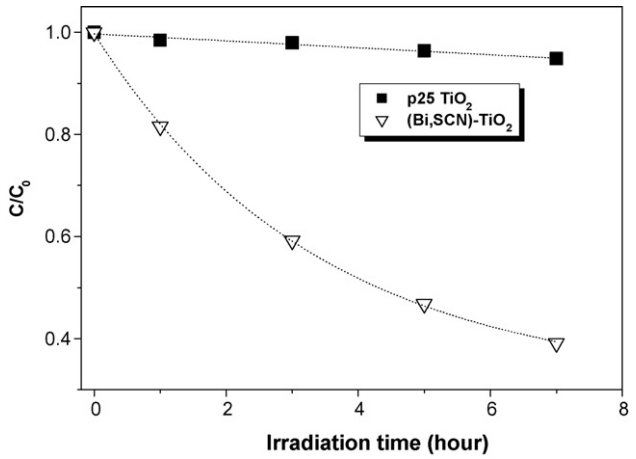

Fig. 8. Kinetics of degradation of phenol (1.0×10^{-4} mol/l, pH 2.0) under visible light ($\lambda > 420$ nm) irradiation.

The doping of TiO_2 with anion, SCN^-, resulted in the lattice defects, such as oxygen vacancies, which enhanced the visible light absorptive capability further (Fig. 4). Oxygen vacancies have been demonstrated by electron spin resonance (ESR) measurements in N doped TiO_2, and the study of Ihara showed that it is the oxygen vacancies that contribution to the Vis activity in N-doped TiO_2 [24]. A recent study by Serpone has also proposed the formation of oxygen vacancies and thus the advent of color centers (e. g., **F**, **F+**, **F++** and **Ti^{3+}**) were responsible for the absorption of the visible light in anions (N, C, and S mostly) doped TiO_2 [25].

It should be noted that dyes, such as RhB, can also be degraded through photosensitization pathway. In that case, it is the dye rather than TiO_2 was excited under the irradiated of light with energy smaller than the band gap of TiO_2. But the degradation of the dye by photosensitizing is much slower than photocatalytic degradation pathway.

4. Conclusions

The goals both of extending the TiO_2 spectral response to the visible region and of improving its photocatalytic activity are realized by modification with $BiCl_3$ and KSCN. The photocatalyst shows much higher photoreactivity than p25 TiO_2 on the degradation of organic pollutants (RhB and phenol) both under UV and visible light irradiation. Doping of TiO_2 with Bi^{3+} resulted in the formation of Bi_xTiO_y, and the heterojunction effects of Bi_xTiO_y/TiO_2 maybe responsible for the higher photoreactivity of Bi^{3+} doped TiO_2. However, lattice defects, such as oxygen vacancies, may be formed in the presence of SCN^-. Doping of TiO_2 with Bi^{3+} and SCN^- enhanced the separation of the carriers (electron and holes) and light absorptive capability, and thus the photoreactivity. The special physical properties also contributed to the high photoreactivity of (Bi,SCN)-TiO_2.

Acknowledgements

The authors are grateful to the Natural Science Foundation of China (20577070) and Science Foundation of South-Central University for Nationalities (YZZ06019) for funding received.

References

[1] T.L. Thompson, J.T. Yates, Surface science studies of the photoactivation of TiO_2-new photochemical processes, Chem. Rev. 106 (2006) 4428–4453.
[2] K.L. Lv, Y.M. Xu, Effects of polyoxometalate and fluoride on adsorption and photocatalytic degradation of organic dye X3B on TiO_2, J. Phys. Chem. B 110 (2006) 6204–6212.
[3] J.G. Yu, J.F. Xiong, B. Cheng, Y. Yu, J.B. Wang, Hydrothermal preparation and visible-light photocatalytic activity of Bi_2WO_6 powders, J. Solid State Chem. 178 (2005) 1968–1972.
[4] J.C. Yu, J.G. Yu, W.K. Ho, Z.T. Jiang, L.Z. Zhang, Effects of F^- doping on the photocatalytic activity and microstructures of nanocrystalline TiO_2 powders, Chem. Mater. 14 (2002) 3808–3816.
[5] R. Asahi, T. Morikawa, T. Ohwaki, K. Aoki, Y. Taga, Visible-light photocatalysis in nitrogen-doped titanium oxides, Science 293 (2001) 269–271.
[6] T. Umebayashi, T. Yamaki, H. Itoh, K. Asai, Band gap narrowing of titanium dioxide by sulfur doping, Appl. Phys. Lett. 81 (2002) 454–456.
[7] S.U.M. Khan, M. Al-Shahry, W.B. Ingler, Efficient photochemical water splitting by a chemically modified *n*-TiO_2, Science 297 (2002) 2243–2245.
[8] X. Hong, Z. Wang, W. Cai, F. Lu, J. Zhang, Y. Yang, N. Ma, Y. Liu, Visible-light-activated nanoparticle photocatalyst of iodine-doped titanium dioxide, Chem. Mater. 17 (2005) 1548–1552.
[9] H. Luo, T. Takata, Y. Lee, J. Zhao, K. Domen, Y. Yan, Photocatalytic activity enhancing for titanium dioxide by co-doping with bromine and chlorine, Chem. Mater. 16 (2004) 846–849.
[10] D. Dvoranova, V. Brezova, M. Mazur, M.A. Malati, Investigations of metal-doped titanium dioxide photocatalysts, Appl. Catal. B-Environ. 37 (2002) 91–105.
[11] S.T. Martin, C.L. Morrison, M.R. Hoffmann, Photochemical mechanism of size-quantized vanadium-doped TiO_2 particles, J. Phys. Chem. 98 (1994) 13695–13704.
[12] X.Y. Li, P.L. Yue, C. Kutal, Synthesis and photocatalytic oxidation properties of iron doped titanium dioxide nanosemiconductor particles, New J. Chem. 27 (2003) 1264–1269.
[13] H.S. Zuo, J. Sun, K.J. Deng, R. Su, F.Y. Wei, D.Y. Wang, Preparation and characterization of Bi^{3+}-TiO_2 and its photocatalytic activity, Chem. Eng. Technol. 30 (2007) 577–582.
[14] W.Y. Choi, A. Termin, M.R. Hoffmann, The role of metal ion dopants in quantum-sized TiO_2: correlation between photoreactivity and charge carrier recombination dynamics, J. Phys. Chem. 98 (1994) 13669–13679.
[15] W. Zhao, W.H. Ma, C.C. Chen, J.C. Zhao, Z.G. Shuai, Efficient degradation of toxic organic pollutants with $Ni_2O_3/TiO_{2-x}B_x$ under visible irradiation, J. Am. Chem. Soc. 126 (2004) 4782–4783.
[16] T. Kako, Z.G. Zou, M. Katagiri, J.H. Ye, Decomposition of organic compounds over $NaBiO_3$ under visible light irradiation, Chem. Mater. 19 (2007) 198–202.
[17] X.P. Lin, T. Huang, F.Q. Huang, W.D. Wang, J.L. Shi, Photocatalytic activity of a Bi-based oxychloride Bi_3O_4Cl, J. Phys. Chem. B 110 (2006) 24629–24634.
[18] W.F. Yao, H. Wang, X.H. Xu, S.X. Shang, Y. Hou, Y. Zhang, M. Wang, Synthesis and photocatalytic property of bismuth titanate $Bi_4Ti_3O_{12}$, Mater. Lett. 57 (2003) 1899–1902.
[19] L.Q. Jing, X.J. Sun, B.F. Xin, B.Q. Wang, W.M. Cai, H.G. Fu, The preparation and characterization of La doped TiO_2 nanoparticles and their photocatalytic activity, J. Solid State Chem. 177 (2004) 3375–3382.
[20] K.S. Kim, N. Winograd, X-ray photoelectron spectroscopic studies of nickel–oxygen surfaces using oxygen and argon ion-bombardment, Surf. Sci. 43 (1974) 625–643.
[21] J.A. Wang, R. Limas-Ballesteros, Quantitative determination of titanium lattice defects and solid-state reaction mechanism in iron-doped TiO_2 photocatalysts, J. Phys. Chem. B 105 (2001) 9692–9698.
[22] Y.Q. Zheng, E.W. Shi, S.X. Cui, W.J. Li, X.F. Hu, Hydrothermal preparation and characterization of brookite-type TiO_2 nanocrystallites, J. Mater. Sci. Lett. 19 (2000) 1445–1448.
[23] Y. Bessekhouad, D. Robert, J. Weber, Photocatalytic activity of Cu_2O/TiO_2, Bi_2O_3/TiO_2 and $ZnMn_2O_4/TiO_2$ heterojunctions, Catal. Today 101 (2005) 315–321.
[24] I. Nakamura, N. Negishi, S. Kutsuna, et al., Role of oxygen vacancy in the plasma-treated TiO_2 photocatalyst with visible light activity for NO removal, J. Mol. Catal. A: Chem. 161 (2000) 205–212.
[25] N. Serpone, Is the band gap of pristine TiO_2 narrowed by anion- and cation-doping of titanium dioxide in second-generation photocatalysts, J. Phys. Chem. B 110 (2006) 24287–24293.